Investigation of a microfluidic approach to study very high nucleation rates involved in precipitation processes

Youen Vitry, Sébastien Teychené, Sophie Charton, Fabrice Lamadie, Béatrice Biscans

▶ **To cite this version:**

Youen Vitry, Sébastien Teychené, Sophie Charton, Fabrice Lamadie, Béatrice Biscans. Investigation of a microfluidic approach to study very high nucleation rates involved in precipitation processes. Chemical Engineering Science, 2015, 133, pp.54-61. 10.1016/j.ces.2015.01.062 . hal-01904656

HAL Id: hal-01904656
https://hal.science/hal-01904656v1

Submitted on 25 Oct 2018

HAL is a multi-disciplinary open access archive for the deposit and dissemination of scientific research documents, whether they are published or not. The documents may come from teaching and research institutions in France or abroad, or from public or private research centers.

L'archive ouverte pluridisciplinaire **HAL**, est destinée au dépôt et à la diffusion de documents scientifiques de niveau recherche, publiés ou non, émanant des établissements d'enseignement et de recherche français ou étrangers, des laboratoires publics ou privés.

OATAO

Open Archive Toulouse Archive Ouverte

OATAO is an open access repository that collects the work of Toulouse researchers and makes it freely available over the web where possible

This is an author's version published in: http://oatao.univ-toulouse.fr/20590

To cite this version:

Vitry, Youen and Teychene, Sébastien and Charton, Sophie and Lamadie, Fabrice and Biscans, Béatrice *Investigation of a microfluidic approach to study very high nucleation rates involved in precipitation processes.* (2015) Chemical Engineering Science, 133. 54-61. ISSN 0009-2509

Any correspondence concerning this service should be sent to the repository administrator: tech-oatao@listes-diff.inp-toulouse.fr

Investigation of a microfluidic approach to study very high nucleation rates involved in precipitation processes

Youen Vitry [a], Sébastien Teychené [a,*], Sophie Charton [b], Fabrice Lamadie [b], Béatrice Biscans [a]

[a] Université de Toulouse, CNRS, INPT, UPS, Laboratoire de Génie Chimique UMR 5503, 4, Allée Emile Monso, F-31030 Toulouse, France
[b] CEA, DEN, F-30207 Bagnols-sur-Cèze, France

HIGHLIGHTS

- Fast nucleation rates were measured in a droplet-based microfluidic system.
- The nucleation rate of neodymium oxalate is found to increase with time.
- The chip design enables to decouple nucleation from mixing.
- Huge supersaturation ratio can be reached without nucleation.

ABSTRACT

A microfluidic device has been specially developed to enable the study of fast nucleation kinetics involved in precipitation processes. This setup allows drops of two different reagents to be generated synchronously and to coalesce, and ensure the mixing of their reactants within few milliseconds. The results presented in this paper show that droplet based microfluidic devices are promising tools for studying high nucleation rates involved in precipitation processes. By using the stochastic nature of the nucleation process and the effect of the confinement on the induction time, a tailored microfluidic device has been used to measure nucleation rates as high as $J = 7.68 \times 10^{13}\ m^{-3}\ s^{-1}$. Moreover, kinetic data deriving from nucleation experiments were found in good agreement with data deriving from "conventional" technics.

1. Introduction

As introduced by Söhnel and Garside (1992), precipitation is a fast crystallization process, taking place at very high supersaturation. As a result, very high number (from 10^{10} to 10^{16}) of small crystals (from 10 nm to 10 μm) are produced. Moreover, as precipitation usually results from a fast chemical reaction, the role of mixing is of paramount importance (Söhnel and Garside, 1992; Baldyga and Orciuch, 2001). Because precipitation processes are prevalent in many chemical industries, a large amount of studies in the literature deal with the determination of the nucleation kinetics, growth rates, aggregation and agglomeration rates involved in these processes (Roelands et al., 2006). It appears from the literature review that the main and more relevant experimental technique to measure nucleation rates, relies on rapid mixers (vortex mixers like Hartridge–Roughton mixers, or *T* mixers) that achieve mixing time as low as a few hundred of microseconds. This low mixing time is assumed to be lower than the induction time required for nucleus formation in the supersaturated solution (which is typically around 1 ms or lower), and nucleation rates are derived from the number of particles produced. The latter can be determined either by optical techniques (*i.e.* a laser measuring the scattered light at the outlet of the mixer) or by quenching the suspension in a gel, in order to prevent further nucleation or crystal growth before counting the crystals (Bertrand-Andrieu et al., 2004; Lindenberg and Mazzotti, 2010). Both approaches are effective, and have generated most of the results available in the literature, but they are product consuming, and thus inappropriate for high added value products or for dangerous species like in the nuclear industry. In addition, because the crystals are analyzed a long time after their generation, relevant information regarding the nucleation process can hardly be derived from the final properties of these crystals.

In the last decade, microfluidic systems have proven to be reliable experimental tools for studying nucleation kinetics of proteins (Shim et al., 2007; Akella et al., 2014), salts (Laval et al., 2007), organic molecules (Dombrowski et al., 2007; Teychene and

Biscans, 2012). In these studies, the authors have used microfluidic systems to generate monodispersed droplets, each of them containing both the solvent and the solute to crystallize, and both flowing in an inert fluid. Supersaturation inside the droplets was generated by cooling down the system below the solubility temperature. The number of empty droplets and of droplets in which one or several crystals are present is then monitored over time. Assuming nucleation is a stochastic process, it can be described by a Poisson distribution (Pound and La Mer, 1952; Goh et al., 2010), from which kinetic can be derived. These works revealed that microfluidic is a powerful technique for studying nucleation. However, only "slow nucleation processes", in which mixing is not critical and occurring at low supersaturation ratio ($S=C/C_{sat}<20$), have been examined.

The present work focuses on the relevance of microfluidic tools for studying the high nucleation rates encountered in reactive precipitation. A specific microfluidic configuration was designed and used to measure nucleation kinetics in the case of oxalates precipitation, as implemented in hydrometallurgical processes, and as recently studied by Charton et al. (2013). The main idea of this study is to take advantage of the increase of the induction time with the decrease of the solution volume V. Indeed, according to the classical nucleation theory, the induction time (*i.e.* the time needed for the first crystal to appear in a supersaturated solution), scales with V^{-1}, meaning that if the solution volume is low enough, the time-scales for the nucleation and mixing processes can be separated. For instance, based on the nucleation kinetics of neodymium oxalate measured with the classical "rapid-mixer" methodology (Bertrand-Andrieu et al., 2004) assuming a typical supersaturation ratio of $S=29$, and according to Chen et al. (2012), a simple calculation yields mean induction times of 1 μs and of 250 ms for solution volume V of 1 ml and 1 nl, respectively. Consequently, a microfluidic chip has been designed to (i) generate droplets with volume ranging from 0.5 nl to 1 nl, (ii) achieve quick mixing of the reactants inside the droplets after their fusion ($t_{mix}\sim 10$ ms), and (iii) ensure proper flow of the droplets in all parts of the system and at all time (*i.e.* to avoid channel clogging). To attest the relevance of this setup for the experimental investigation of fast nucleation events at high supersaturation ratio, two important issues must be addressed: Can nucleation be efficiently decoupled from mixing? Is it still possible to observe and to measure the stochastic nature of the nucleation process?

2. Material and methods

2.1. Fluids and reagents

Regarding the precipitation experiments, the following fluids and reagents were purchased from Sigma Aldrich: Neodymium nitrate hexahydrate ($2Nd(NO_3)_3$, $6H_2O$, purity: 99.9%), oxalic acid dihydrate ($H_2C_2O_4$, $2H_2O$, purity > 99.5%), nitric acid (HNO_3, 70%), 1*H*–1*H*–2*H*–2*H* perfluorodecyltrichlosilane (FDTS, purity: 97%), 1*H*,1*H*,2*H*,2*H*-perfluoro-1-octanol (PFO, purity: 97%), 2,2,4-trimethylpentane (purity > 99.5%).

Regarding specific materials required for the chips' production: Norland Optical Adhesive N°81 (NOA-81) was purchased from Edmund Optics; Polydimethyl siloxane (PDMS) was purchased from Ellsworth Adhesive Europe and SU8 2150 was purchased from Microchem.

All the reagents were used without further purification.

2.2. Interfacial and surface tension measurements

Interfacial tension was measured with a commercial drop shape analysis system (DSA100S, Krüss), equipped with camera. DSA software fits the digital drop profile to a numerical solution of the Young–Laplace equation. 50 μl Hamilton syringes (Harvard Apparatus) pre-filled with the fluorinated oil and perfluorooctanol were used to produce 2 μl hanging drops on the beveled tip of a 22 ga needle (Hamilton) immersed in a glass cell (Hellma), filled with aqueous solution. The measurements were performed at 23 °C.

Contact angle measurements were performed using the same apparatus operated in the sessile drop mode. A droplet of 50 μl was deposited on the surface, and the shape of the droplet was measured using the built-in image treatment software (DSA software). The experiments were performed at 23 °C.

2.3. Design of the microfluidic chips

Fig. 1 presents a schematic of the microfluidic chip that has been built. It is divided into four sections, each one dedicated to a given function.

The first portion is dedicated to the generation and synchronization of a pair of drops, one drop of each reagent. Droplets of each reactant are generated by two T-junction ① allowing a reproducibility of 97% regarding the volume of each droplet (Gu et al., 2011). The pair of droplets is synchronized thanks to a pressure oscillator ② and an oil by-pass ③ (Hong et al., 2010). Indeed, the pressure oscillator allows droplets to be generated alternatively on the one and the other T-junction, while the oil bypass ensures synchronization of the droplets pair by balancing the flow velocity between each channel. The second part consists in a Y-junction ④ wherein droplets coalescence occurs. The details of the hydrodynamic design of the microfluidic chip is similar to the ones found in Hong et al. (2010).

To study nucleation and to decrease the mixing time of the content of the merged drop (Sarrazin et al., 2007), a winding channel ⑤ has been added to the design developed by Hong et al. (2010).

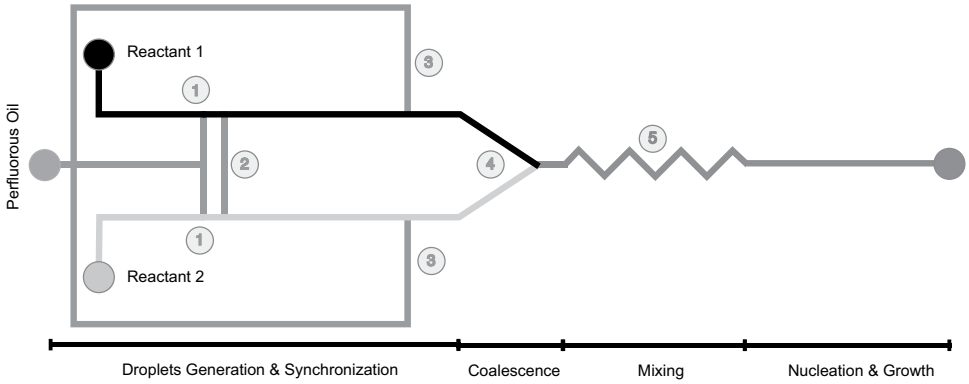

Fig. 1. Schematic of the microfluidic chip design. ① T-junctions; ② pressure oscillator; ③ oil by-pass; ④ Y-junction (droplets fusion); ⑤ winding channels (mixing).

2.4. Chips making

Microfluidics devices were made of NOA-81, a UV-curable polymer. NOA-81 offers a better solvent compatibility than the conventional PDMS, especially with organic solvent (Wägli et al., 2011; Sollier et al., 2011). The process is briefly described hereinafter.

A single layer of epoxy-based negative photoresist (SU-8 2050, microchem, USA) was prepared on a two face–polished wafer (Optics-concept) to obtain 50 μm depth microfluidic master mold by standard photolithography. Briefly, SU-8 was first spin coated onto carefully cleaned silicon wafer at a speed of 3150 rpm. The coated silicon wafer was then ramped slowly from room temperature to 65 °C and maintained for 30 min. The temperature was then slowly increased to 95 °C and maintained for 45 min. At the end of the pre-bake step, the hotplate was turn off allowing the wafer to cool down to room temperature. The wafer is then patterned in contact mode, with a photolithography mask, by UV exposure (UV-KUB, Kloe) with an energy of 175 mJ cm^{-2}. The post exposure bake was performed for 5 min at 65 °C and 15 min at 95 °C, respectively. Development step was operated after the wafer cooled down to room temperature by di-acetone as developing solvent. The final height of the SU-8 wafer, measured by a Zygo optical profilometer, was 50 μm ± 1 μm.

In a second step, a mixture of PDMS and curing agent (Sylgard 184, Down Corning) with a 10:1 ratio was poured on the SU-8 mold after being carefully mixed and degassed in a vacuum chamber. The PDMS was then cured in an oven at 70 °C for at least 2 h. Next, the PDMS mold was peeled off cautiously and put in a vacuum chamber in order to withdraw all the air from the polymer.

Afterwards, microfluidic stickers are obtained according to the procedure described by Bartolo et al. (2008). The required amount of NOA-81 (1 to 2 ml) is poured on a glass substrate. The structured PDMS mold is then gently pressed onto the drop. A small force is applied on the surface of the PDMS mold to be sure that there is no space that NOA-81 cannot reach. In order to absorb the air bubbles stuck between the PDMS and the glass slide, the chip is left at rest for at least 30 min. The NOA-81 is then insulated in the UV-KUB through the transparent PDMS mold for 4 s at 25 mW cm^{-2}. This properly controlled exposure time allows to replicate the microchannels on the bottom substrate while maintaining a very thin layer of uncured NOA-81. This is caused by the presence of oxygen at the PDMS interface, that locally inhibits the free-radical polymerization. A similar procedure is used to produce the cover, except that the exposure time was increased to 120 s at 25 mW cm^{-2}, in order to obtain a rigid surface. Bonding is achieved upon bringing both surfaces into contact, and UV-curing for 120 s at 25 mW cm^{-2} of the above mentioned thin layer of uncured NOA-81 on the top surface. This leads to a permanently sealed microchannel. The use of a NOA cover instead of a standard glass cover guarantees that all the walls have the exact same wettability. The fluidic channels obtained have a square cross section of 50 × 50 μm^2.

Nanoports (IDEX Health and Science) are then glued over the channels inputs and output with a standard epoxy glue (3 M Scotch Weld DP 105). The glue is cured in an oven at 65 °C for 1 h.

2.5. Surface treatment

The silanization process is achieved in a glove box (Erlab) under nitrogen inert atmosphere. Prior to the treatment, the NOA microfluidic channels are carefully cleaned by flowing ethanol and 2,2,4-trimethylpentane at a flow rate of 200 μl h^{-1} for 30 min. The channels were then filled with a 1.5% v/v mixture of FDTS and 2,2,4-trimethylpentane. After 15 min of incubation, the FDTS excess is removed by successively flushing the channel with isooctane and isopropanol, each for 20 min. At last, the device is dried overnight at 65 °C.

To examine the effects of the surface modification, glass slides were also coated with NOA-81 and exposed to UV irradiation for 2 min at 25 mW cm^{-2}. The surface modification protocol was the same as for the channel. To ensure that the siliconized surface keeps its properties over time and when exposed to different environment, the glass slides were put in contact to solutions used in the experiments. The data obtained are presented in Table 1. The results are consistent with the ones obtained by Gu et al. (2010). In addition, the long-term stability of the FDTS layer appears very good, as evidenced by the minor variations in contact angle observed after 1 to 5 days of exposure to either air, water, acid or oil phase.

2.6. Experimental setup

The flow-rates are controlled using a Nemesys syringe pump (Cetoni) with a precision of ± 0.001 μl min^{-1}. For all experiments, a 0.1% v/v mixture of Fluorinated Oil FC-40 (3 M) with PFO is used as the continuous phase.

Droplets generation and coalescence studies were performed using ultra-pure water (Ω = 18.2 MΩ cm^{-1}) as the dispersed phase.

For studying mixing inside droplets, methylene blue (50×10^{-3} M) was used as dye. These experiments were performed by fusing droplets containing the methylene blue dye with pure water droplets.

For hydrodynamic characterization, the volumetric flow-rate ranges from 5 to 20 μl min^{-1} and from 0.5 to 2 μl min^{-1} for the oil and the aqueous solution, respectively.

A microscope (Zeiss Axio-observer A1) equipped with a fast camera (SA3, Photron) is used to record images at a rate of 2000 frames per seconds (fps) with an exposure time of 25 μs. Image processing was performed using a specific algorithm developed in Matlab® environment (Mathworks, Cambridge, UK). Briefly, the droplets are identified and detected using a normalized cross-correlation function available in Matlab. This function recognizes, from template images, the nose and the tail of the droplet. Then, a tracking algorithm keeps track of individual droplets by finding drops which partially overlap the successive images. This results in a sequence of isolated and labeled droplets. This algorithm is used to measure the size (length of the plug) and size distribution of the droplets, the inter-droplet length, and the droplet generation frequency. Assuming the droplet shape is a geoid, the volume can be derived from the length of the droplet and the channel dimensions (width and height).

To quantify the mixing inside the droplets, we couple this tracking algorithm with an algorithm previously developed by Sarrazin et al. (2007). Briefly, the standard deviation of the gray value of homogenous droplets containing dye at a known concentration are first determined, in order to correct the inhomogeneity due the illumination and the presence of the interface. The mixing degrees of the dye and water in a droplet after coalescence are then quantified by comparing the evolution of its standard deviation with the one obtained for the homogeneous drop of the same dye concentration. The fused-droplet value approaches the reference one as the mixing process goes on. The mixing stage of a droplet at a given time t is represented by the dimensionless number χ, characteristic of the heterogeneities in gray value inside the droplet, and is calculated from:

$$\chi = \frac{\overline{\sigma^t} - \overline{\sigma^{ref}}}{\overline{\sigma^0} - \overline{\sigma^{ref}}} \quad (1)$$

Table 1
Contact angles measurements for aqueous drops on NOA-81 surfaces.

Time after treatment	1 Day	5 Day	1 Day	1 Day	1 Day
Aging environment	Air	Air	water	1 M HNO_3	FC40
Contact angle	113 ± 2°	111 ± 3°	110 ± 2°	110 ± 2°	111 ± 2°

where $\overline{\sigma^0}$, $\overline{\sigma^t}$, $\overline{\sigma^{ref}}$ are the mean standard deviation of the gray value in the whole droplet initially, at time t, and of the reference droplet, respectively.

3. Results and discussion

3.1. Hydrodynamic characterization

3.1.1. Generating pairs of droplets

The system capability for generating the aqueous droplets was investigated in a wide range of flow conditions, with flow-rates ranging from 5 to 20 μl min^{-1} and from 0.5 to 2 μl min^{-1} for the continuous, and dispersed phases, respectively. It was observed that monodispersed droplets are generated with a variation coefficient lower than 2%. The droplet size and the corresponding volume are plotted in Fig. 2b. The volume of the obtained droplets ranges from 0.15 to 0.55 nl.

In addition, as depicted by Fig. 2a and b, the droplets generation frequencies and the droplet sizes are the same for each channel, whatever the flow-rate ratio Q_d/Q_c between both phases. Droplets frequency in the range 20 to 160 Hz have been achieved. For the sake of illustration, with a water flow-rate of 2 μl min^{-1} and an oil flow-rate of 10 μl min^{-1}, the generation of 1000 independent droplets requires only 10 s and a total amount of solution of only 0.67 μl.

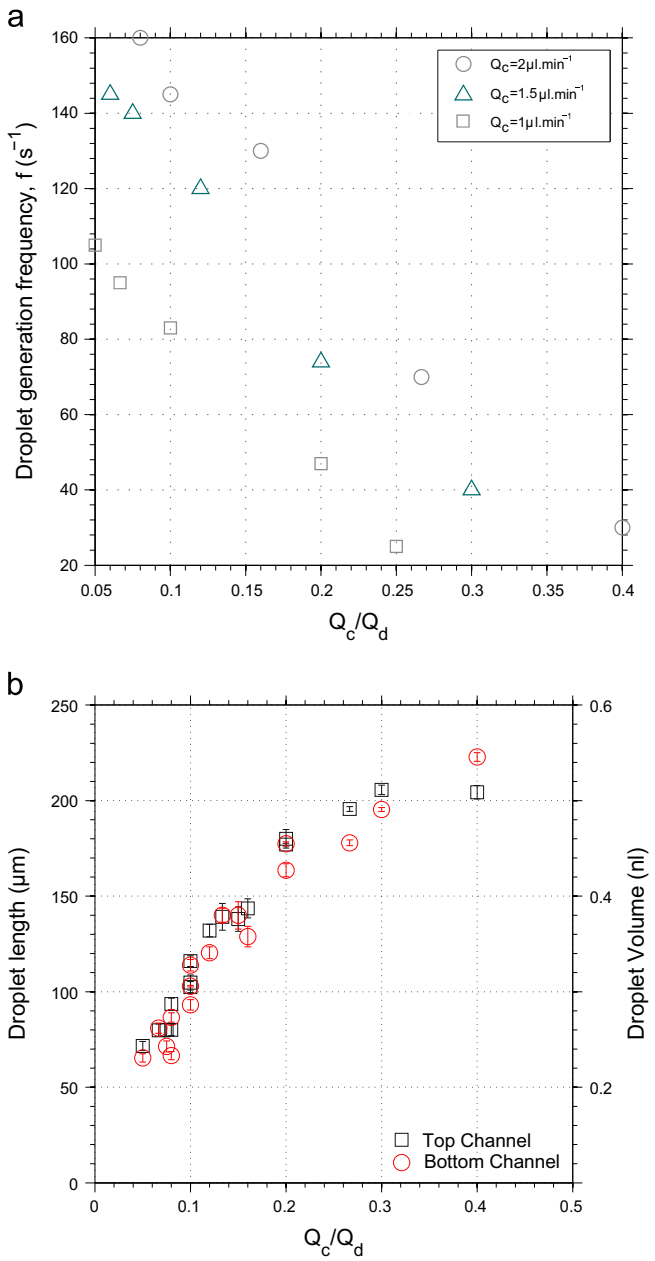

Fig. 2. Hydrodynamic characterization of the droplet generation. (a) Droplet volume as function of the flow rate ratio–(b) Droplet generation frequency *vs.* flow rate ratio.

3.1.2. Droplets synchronization and fusion

Droplet coalescence is one of the most important steps of this approach. Efficient coalescence of surfactant-stabilized droplets is indeed challenging. Mazutis and Griffiths (2012) have shown that the fusion efficiency of passive droplets generated on-chip is critically dependent of both the contact time, τ, between the droplets, prior to the coalescence event, and of the surface coverage by the surfactant, Γ. Droplets coalesce selectively only when τ is above a critical time and when Γ is lower than ~66%.

The relation between the bulk surfactant concentration, c, and the interfacial coverage, Γ, can be described by a Langmuir isotherm (Danov et al., 1999):

$$\Gamma = \Gamma_\infty \frac{c}{c+B} \tag{2}$$

where Γ_∞ is the saturating surfactant concentration at the interface and B is the Langmuir constant. The amount of surfactant adsorbed per unit of area is related to the interfacial tension and to the surfactant concentration by the Gibbs equation of adsorption:

$$d\Upsilon = -RT\sum_i \Gamma_i \ln c_i \tag{3}$$

where T is the absolute temperature, R the gas constant and c_i the concentration of species i in the mixture.

The Szyszkowski equation (Danov et al., 1999) relating the interfacial tension with the concentration is obtained by

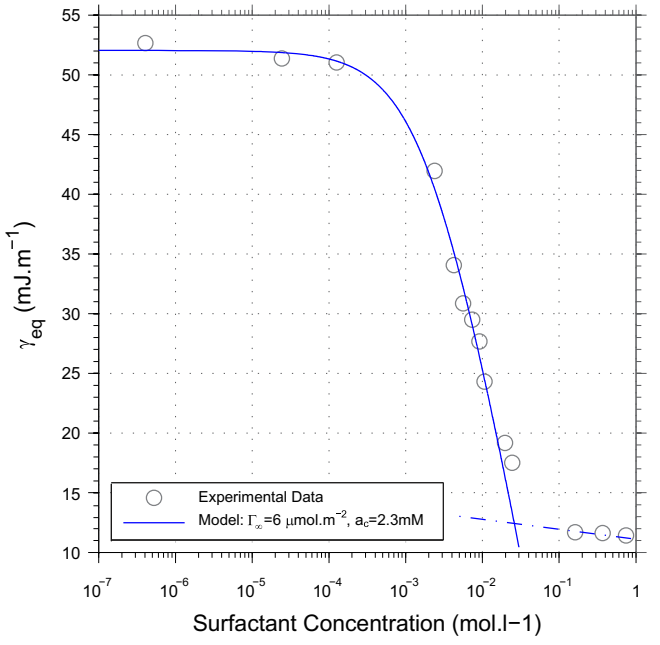

Fig. 3. Evolution of the "FC40/water" equilibrium interfacial tension with the PFO concentration. The red line stands for Langmuir adsorption model (Eq. (2)) and the black circles for the experimental data. (For interpretation of the references to color in this figure legend, the reader is referred to the web version of this article.)

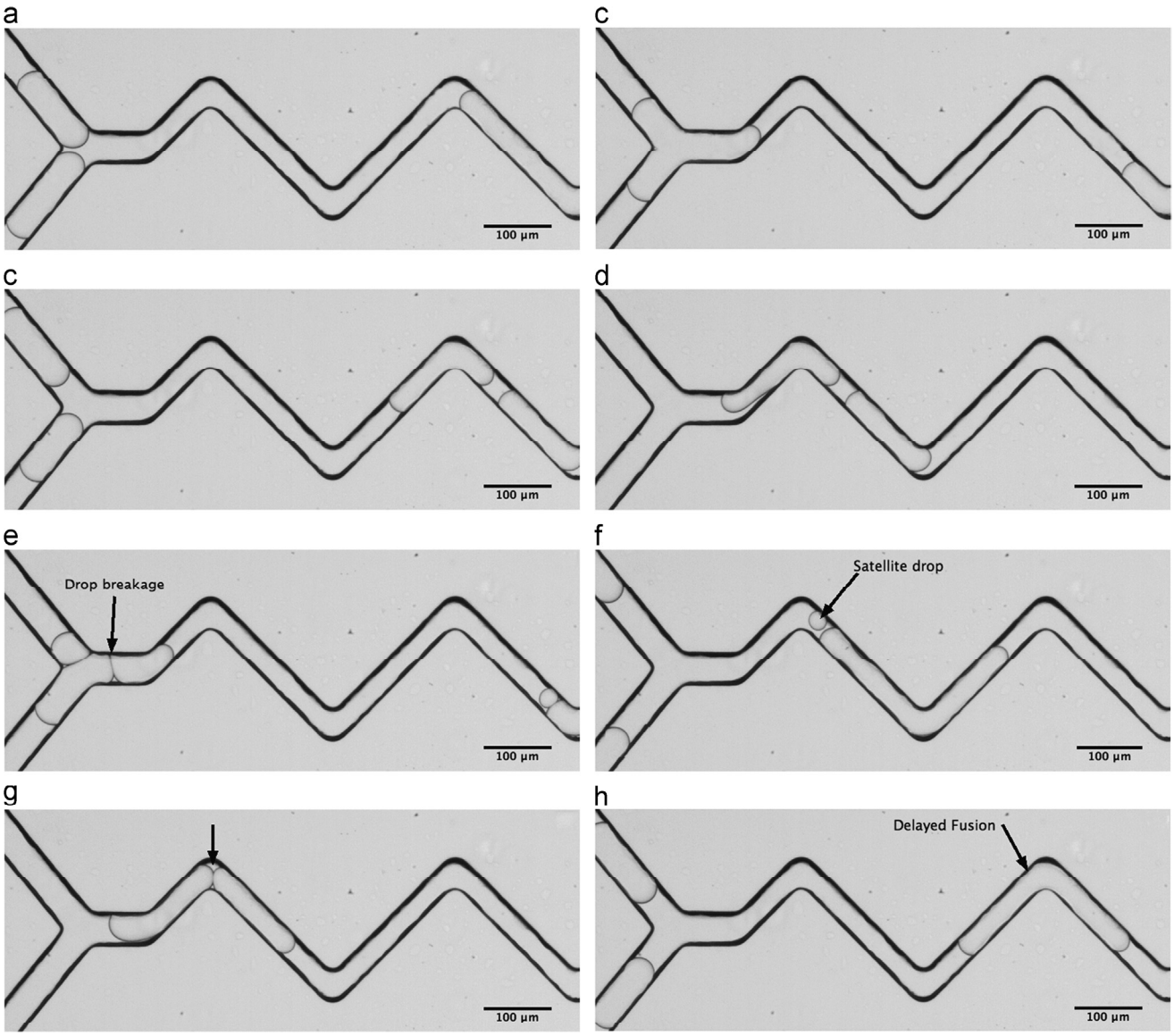

Fig. 4. Photographs of droplet coalescence events inside the microfluidic channel. From left to right and from top to bottom: (a)–(b) Effective coalescence; (c)–(d) desynchronization of the droplets; (e)–(f) droplet breakage (long plugs) (g)–(h) uncontrolled coalescence (c=0.5% (v/v), $\Gamma > 66$ %).

integrating Eq. (3) along with Eq. (2):

$$\pi_s = \gamma - \gamma_0 = -RT\Gamma_\infty \ln\left(1+\frac{c}{B}\right) \tag{4}$$

where π_s is the interfacial pressure, γ and γ_0 are the interfacial tensions of the pure solvent and of the mixture, respectively.

By combining Eqs. (3) and (4) and eliminating c, one obtain the Frumkin equation of state:

$$\Gamma(t) = \Gamma_\infty\left[1-\exp\left(-\frac{\gamma_0-\gamma}{RT\Gamma_\infty}\right)\right] \tag{5}$$

For the system under study, Γ_∞ has been determined from equilibrium interfacial tension values γ_{eq} measured by the pendent drop technique at various surfactant concentrations c (Fig. 3). Numerical identification of the experimental values according to Eq. (4) results in $\Gamma_\infty = 6.26 \times 10^{-6}$ mol m^{-2} and $B = 2.3 \times 10^{-3}$ M. Accordingly, and following Eq. (5), the 66%-threshold interface coverage is reached for a concentration of 0.1% (v/v) of PFO in FC40 and an interfacial tension of 32 mN m^{-1}.

However, unlike the observations of Hong et al. (2010) efficient droplet fusion (illustrated by Fig. 4a and b) is achieved only for a very limited range of operating conditions in our microfluidic system. Indeed, several pathologies have been observed:

- for high values of the flow-rate ratio Q_d/Q_c, non-synchronized droplets are observed as depicted in Fig. 4c and d;
- in some cases (Fig. 4e and f), the droplets are synchronized but split during the fusion process, leading to droplets of uncontrolled volume;
- in other cases, the fusion of the droplets occurs in the wedging channel (for an interfacial coverage higher than 66%, Fig. 4g and h).

However, with an aqueous flow-rate of 2 µl min^{-1} and an organic flow-rate ranging from 7.5 to 10 µl min^{-1}, and for a surfactant concentration of 0.1% (v/v), it has been reproducibly observed that at least 95% of the droplets coalesce few milliseconds after leaving the Y-junction (Fig. 4a).

3.1.3. *Droplet mixing*

Mixing times were measured after the coalescence between droplets containing water and methylene blue. All the droplets

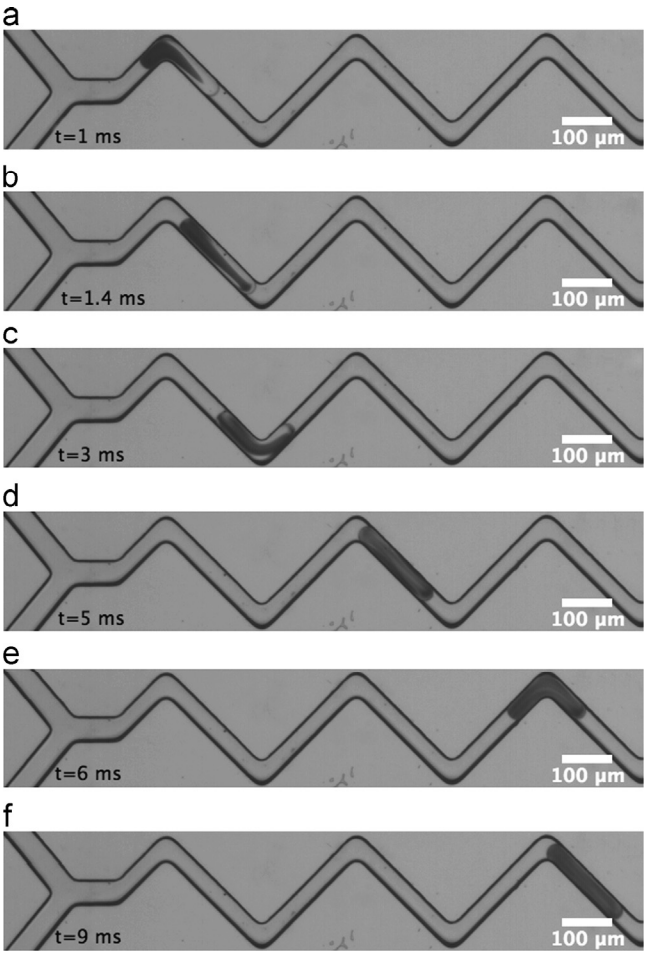

Fig. 5. Droplet mixing evolution after coalescence: (a) $t=0$ ms (b) $t=0.4$ ms (c) $t=2$ ms (d) $t=4$ ms (e) $t=6$ ms (f) $t=9.5$ ms.

have been generated at the same conditions and reach the entrance of the winding channel within less than 1 ms after coalescence. At this position which corresponds to the initial mixing time, all the analyzed droplets have the same "Janus"- like fluid orientation. They are separated into two hemispheres containing the dye and the water, as shown in Fig. 5a.

The time-evolution of the mixing criteria defined in Eq. (1), after coalescence, is plotted in Fig. 6 for different flow rates of the continuous and dispersed phases, respectively. For all the flow rates tested, a rapid decrease of the mixing criteria is observed.

For each point, hundreds of droplets were analyzed and it was found that the mixing parameter is reproducible and similar for all the droplets. Typical images of droplet mixing are presented in Fig. 5.

From these experiments, typical mixing times of 12 ms and 7 ms were evidenced for a continuous phase flow rate of 10 µl min^{-1} and 20 µl min^{-1}, respectively. As shown in Table 2, these results are in good agreement with the theory of chaotic mixing (Capretto et al., 2011):

$$t_{theo} \sim \frac{aw}{u} \log(Pe) \tag{6}$$

where w is the channel width, a is the droplet length normalized by the channel width w, and Pe stands for the Peclet number depending on the diffusion coefficient D:

$$Pe = \frac{wu}{D} \tag{7}$$

The mixing time obtained from experimental values and from Eq. (6) are compared in Table 2.

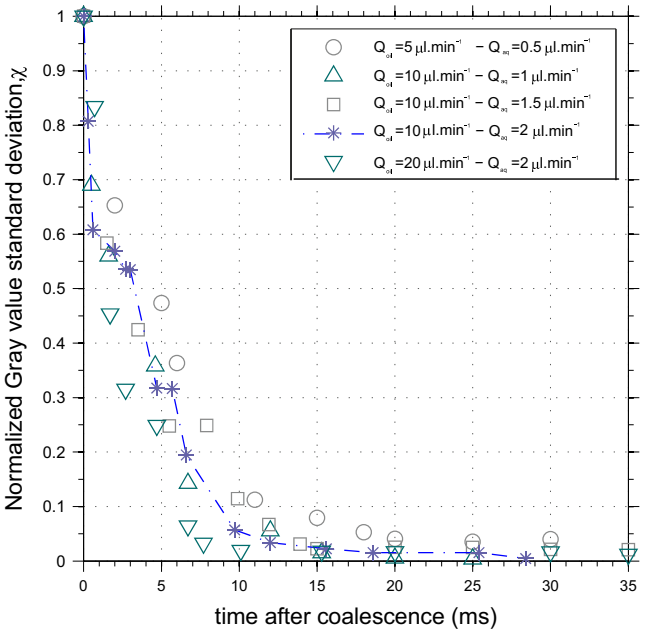

Fig. 6. Temporal evolution of the mixing criteria in the winding channel for different flow rates of the dispersed and continuous phases.

Table 2
Evolution of the mixing time for different flow-rates in the winding channel after coalescence.

Q_c (µl min^{-1})	5		10		20
Q_d (µl min^{-1})	0.5	1	1.5	2	2
t_{exp} (ms)[a]	20	12	13	13	8
t_{theo} (ms)[b]	~20	~11	~12	~13	~7

[a] The mixing time was determined when $\chi < 5\%$, which correspond to the standard deviation of the homogenous droplet.
[b] The diffusion coefficient of methylene blue in water is $D = 0.8 \times 10^{-9}$ m^2 s^{-1}.

3.2. Nucleation experiments

Nucleation experiments were performed by fusing droplets containing neodymium nitrate dissolved in nitric acid (1.5 M HNO_3 and 0.08 M $Nd(NO_3)_3$) with droplets of oxalic acid (0.7 M). Neodymium oxalate crystals are formed according to the following reaction:

$$2Nd(NO_3)_3 + 3H_2C_2O_4 \rightarrow Nd_2(C_2O_4)_3 + 6HNO_3$$

A Pitzer model was used to compute the activity coefficients of the species, yielding a supersaturation ratio, defined by Eq. (8), of $S=29$[1] with the aforementioned concentrations.

$$S = \left(\frac{a^2_{Nd^{3+}} a^3_{C_2O_4^{2-}}}{K_{sp}} \right)^{1/5} = \left(\frac{a^2_{Nd^{3+}} a^3_{C_2O_4^{2-}}}{a^2_{Nd^{3+},eq} a^3_{C_2O_4^{2-},eq}} \right)^{1/5} \tag{8}$$

The value of the solubility product, K_{sp}, ($K_{sp,} = 1.3 \times 10^{-31}$) is taken from the work of Chung et al. (1998). The detailed calculation of the Pitzer interaction parameters and the corresponding activity coefficients are beyond the scope of this paper, and will be published in a dedicated paper. The experimental and modeled

[1] It is worth noting that the supersaturation ratio calculated in the case of ideal solution (*i.e.* by neglecting the activity coefficient in Eq. (8)) is $S = 5.7 \times 10^5$. This order of magnitude of the supersaturation ratio is representative of most of the precipitation processes of insoluble salts.

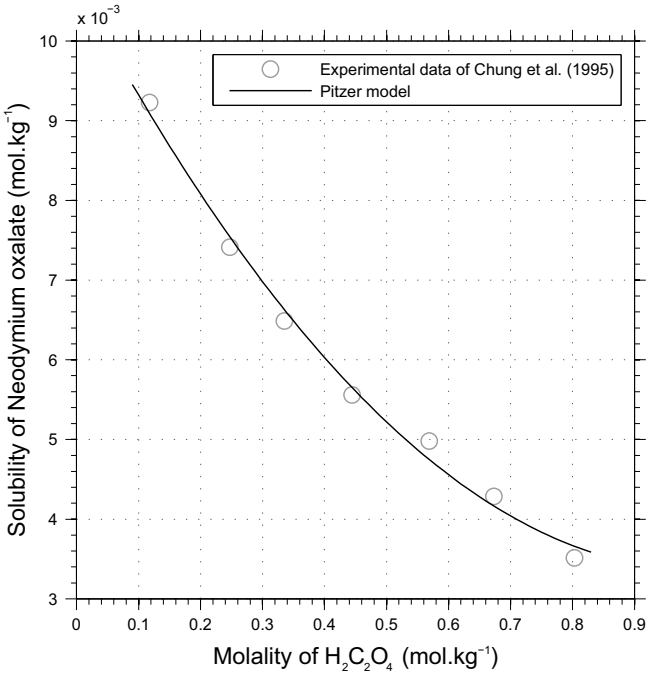

Fig. 7. Solubility of neodymium oxalate in oxalic acid solution in 1 M solution of nitric acid. Experimental data were taken from the work of Chung et al. (1998).

solubility curve of neodymium oxalate in oxalic acid solutions for a concentration of 1 M of nitric acid are presented in Fig. 7.

For these experiments, flow-rates are 2 μl min^{-1} and 10 μl min^{-1}, for the dispersed and continuous phases respectively and correspond to the range of flow-rates of maximum coalescence efficiency at the Y-junction. The droplets have a volume of 0.45 nl each and are generated at a frequency of 90 Hz. Image sequences of 1.2 s, of the flowing droplets were recorded at 10, 50, 75, 100 ms after complete mixing (*i.e.* at 23, 63, 88, 113 ms after coalescence). As an example, pictures taken at different position in the chip are shown in Fig. 8a and b. These images clearly evidence the stochastic nature of the nucleation process. Indeed, for a droplet residence time lower than 50 ms after mixing, only a few numbers of drops contain crystals (3 out of 200 analyzed droplets); whereas for higher residence time, the amount of empty droplets significantly decreases (25% of empty droplets at 100 ms). In addition, from images containing precipitate, no individual crystal can be detected. The precipitate is rather formed by cluster of very small crystals, which is in good agreement with the high supersaturation level inside the droplets. Consequently, in this system, the detection limit of the nucleation threshold, is not the observable size reached by the growth of the crystal (around 2 μm in these setup) but rather the aggregation process between these crystals that modify the optical properties of the solution inside the droplets.

As we already proceed for crystallization (Teychene and Biscans, 2012), the nucleation kinetics of the precipitation process can be obtained from Eq. (9) by counting the number of empty droplets N^G_{empty} as a function of time and assuming that the nucleation process can be described by a Poisson process (Pound and La Mer, 1952):

$$\log\ (P_0) = \log\,(1-P_{nucl}) = \log\ \left(\frac{N^G_{empty}}{N^G_{total}}\right) = -JV_{drop}t \qquad (9)$$

Based on the analysis of some 200 droplets at each position in the chip (totaling 800 droplets), the time-evolution of the proportion of empty droplets is plotted on Fig. 9. Usually, with no pre-existing supernuclei, for homogeneous (pure Poisson process) and heterogeneous nucleation (Poisson process modified by Pound and La Mer (1952)), the evolution of log P_{nucl} should increase linearly with time

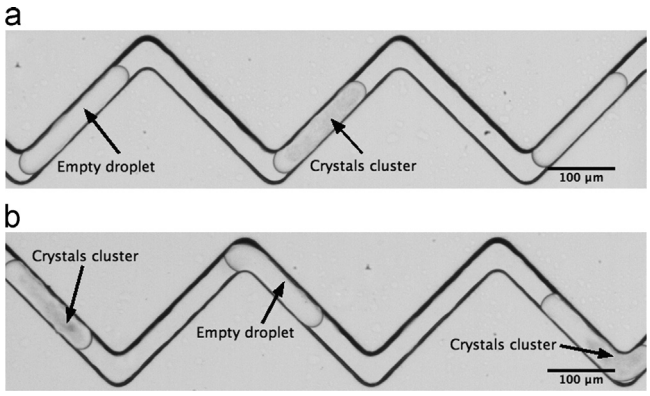

Fig. 8. Images of supersaturated droplets acquired at different position on the microfluidic chip showing the stochastic nature of the nucleation process. (a) $t=50$ ms; the droplet in the center contains precipitate (a cluster of small crystals); (b) $t=100$ ms; Two of the three droplet contains a denser precipitate compared to the one obtained at 50 ms.

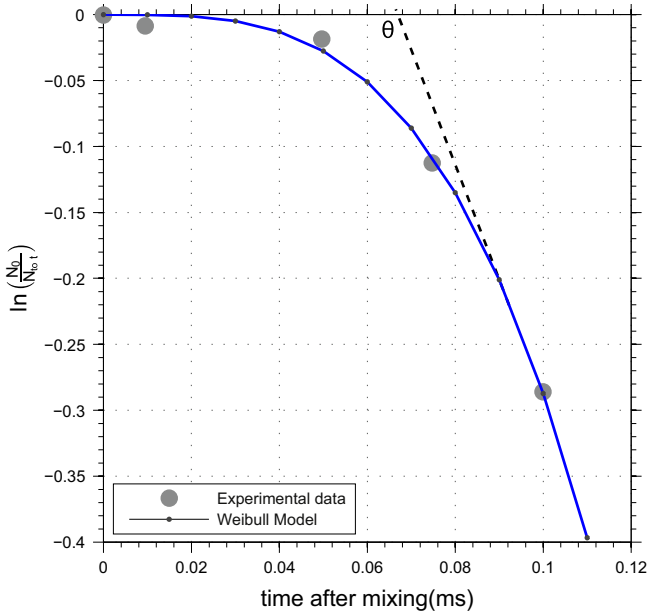

Fig. 9. Temporal evolution of the proportion of empty droplets observed for a supersaturation ratio of $S=29$.

and should start as soon as the solution is supersaturated. However, as shown in Fig. 9, for the case under study, a characteristic time exists, called delay time of nucleation ϑ (Kashchiev, 2000), during which "non-stationary" nucleation occurs at zero rate ($0 \le t \le \vartheta$), while a stationary rate, J, is reached beyond (for $t > \vartheta$). From the intercept value of the asymptote of the log P_{nucl} evolution curve, the delay time for our system is determined $\vartheta = 70$ ms. The origin of the delay time for this system is not clear yet. It can be due to either a non-stationary nucleation process, or to a two-step nucleation mechanism (Kashchiev and Sato, 1998) or to the delay time to detect any optical modification of the solution. Toldy et al. (2012) reported that microdroplets formed by a microfluidic device were not always perfectly separated and they explained that β was larger than unity as a result of nucleation triggered by the surrounding crystallized droplets. In our study, this interpretation can be ruled out because the droplets are flowing continuously and are far enough to avoid overlapping.

Similar behavior of the log(P_0) curve has already been observed in the literature (Kim et al., 2013; Weidinger et al., 2003; Toldy et al., 2012, Boinovich et al., 2014). In all these studies, the log(P_0) curve also starts with a plateau at lower time scale (indicating very little nucleation), and then the nucleation

probability curves decreases, dropping more and more steeply as time increases. The effective nucleation rate is a rapidly increasing function of time. This kind of nucleation behavior belongs to class III of the "Sear classification": increase of the effective nucleation (Sear, 2014). To model the nucleation probability, a Weibull function was chosen, Eq. (10). The Weibull function is a compressed exponential model, characteristic of a non-homogeneous Poisson process.

$$P_{nucl} = \exp\left(-\frac{t}{\tau}\right)^{\beta} \tag{10}$$

The best fit of our experimental data gives $\tau = 0.1446\ s^{-1}$, and $\beta = 3.382$. The large value of β is a consequence of the plateau in the nucleation probability curve followed by a steep drop.

From the slope of the asymptote (at $t > \vartheta$) of the plot in Fig. 9, it is possible to compute the nucleation rate from the following relation:

$$\tau = \frac{1}{JV} \tag{11}$$

The value obtained with a droplet volume of 0.9 nl is $J = 7.68 \times 10^{13}\ m^{-3}\ s^{-1}$.

This value is in fair agreement with previously published values by Plasari and co-workers (*e.g.* Parmentier et al., 2013), using a stopped-flow device equipped with a Hartridge–Roughton confined impinging jet mixing device, in which micromixing is achieved in one millisecond. From their experimental results, the homogeneous nucleation rate is obeying Eq. (12), which gives nucleation rate ranging from 1.11×10^{12} to $1.72 \times 10^{13}\ m^{-3}\ s^{-1}$ at a supersaturation ratio of $S = 29$.

$$J_{HR} = 9.8(\pm 5) \times 10^{19} \exp\left(\frac{-206(\pm 25)}{\ln^2 S}\right) \tag{12}$$

4. Conclusion

The results presented in this paper show that droplet microfluidic devices are very powerful tools for studying high nucleation rates involved in precipitation processes. By using the stochastic nature of the nucleation process and the effect of the confinement on the induction time, we have shown that tailored microfluidic devices can be used to measure nucleation rates as high as $J = 7.68 \times 10^{13}\ m^{-3}\ s^{-1}$.

Moreover, kinetic data deriving from nucleation experiments were found in good agreement with data deriving from "conventional" technics.

Ongoing works is aimed at improving the coalescence efficiency and the automatic image analysis in order to increase the amount of droplets analyzed during the nucleation experiments, and therefrom improve the precision of the nucleation kinetics measurements. In addition, to decrease the detection threshold and find the origin of the plateau observed in the nucleation curves, and to get a better understanding of the nucleation mechanism, it is planned to couple this experimental set-up with online diffusion techniques (Light or X-ray) to analyze to shape and the structure of the cluster observed experimentally.

Acknowledgments

The authors gratefully acknowledge the Fédération de Recherche Fermat and the Nuclear Energy Division of CEA for respectively material and financial supports. We also thank Emmanuel Cid (LGC) for his help on the technical aspects of image acquisition and analysis and Gilles Borda (CEA) for fruitful discussions on the various aspects of oxalate precipitation.

References

Akella, S.V., Mowitz, A., Heymann, M., Fraden, S., 2014. Emulsion-based technique to measure protein crystal nucleation rates of lysozyme. Cryst. Growth Des. 14 (9), 4487–4509.
Baldyga, J., Orciuch, W., 2001. Some hydrodynamic aspects of precipitation. Powder Technol. 121 (1), 9–19.
Bartolo, D., Degré, G., Nghe, P., Studer, V., 2008. Microfluidic stickers. Lab Chip 8, 274–279.
Bertrand-Andrieu, M., Plasari, E., Baron, P., 2004. Determination of nucleation and crystal growth kinetics in hostile environment: application to the tetravalent uranium oxalate $U(C_2O4)_2 \cdot 6H_2O$. Can. J. Chem. Eng. 82, 930–938.
Boinovich, L., Emelyanenko, A.M., Korolev, V.V., Pashinin, A.S., 2014. Effect of wettability on sessile drop freezing: when superhydrophobicity stimulates an extreme freezing delay. Langmuir 30, 1659–1668.
Capretto, L., Cheng, W., Hill, M., Zhang, X., 2011. Micromixing within microfluidic devices. Top. Curr. Chem. 304, 27–68.
Charton, S., Kacem, A., Amokrane, A., Borda, G., Puel, F., Klein, J.-P., 2013. Actinides oxalate precipitation in emulsion modeling: from the drop scale to the industrial process. Chem. Eng. Res. Des. 91, 660–669.
Chen, K., Goh, L., He, G., Kenis, P.J.A., Zukoski III, C.F., Braatz, R.D., 2012. Identification of nucleation rates in droplet-based microfluidic systems. Chem. Eng. Sci. 77, 235–241.
Chung, D.-Y., Kim, E.-H., Lee, E.H., Yoo, J.-H., 1998. Solubility of rare earth oxalate in oxalic and nitric acid media. J. Ind. Eng. Chem. 4 (4), 277–284.
Danov, K.D., Kralchevsky, P.A., Ivanov, I.B., 1999. Properties. In: Dekker, M. (Ed.), Handbook of Detergents, Part A.. CRC Press, New York, pp. 303–418.
Dombrowski, R.D., Litster, J.D., Wagner, N.J., He, Y., 2007. Crystallization of alpha-lactose monohydrate in a drop-based microfluidic crystallizer. Chem. Eng. Sci. 62, 4802–4810.
Goh, L.M, Chen, K.J.n, Bahmidi, V., He, G., Kee, N.C.S., Kenis, P.J.A., Zukoski, C.F., Braatz, R.D., 2010. A stochastic model for nucleation kinteics determination in droplet-based microfluidic systems. Cryst. Growth Des. 10, 2515–2521.
Gu, H., Duits, M.H.G., Mugele, F., 2010. A hybrid microfluidic chip with electrowetting functionality using ultraviolet (UV)-curable polymer. Lab Chip 10 (12), 1550–1556.
Gu, H., Duits, M.H.G., Mugele, F., 2011. Droplets formation and merging in two-phase flow microfluidics. Int. J. Mol. Sci. 12 (4), 2572–2597.
Hong, J., Choi, M., Edel, J.B., deMello, A.J., 2010. Passive self-synchronized two-droplet generation. Lab Chip 10, 2702–2709.
Kashchiev, D., 2000. Nucleation. Butterworth-Heinemann, Burlington.
Kashchiev, D., Sato, K., 1998. Kinetics of crystallization preceded by metastable-phase formation. J. Chem. Phys. 109 (19), 8530–8540.
Kim, J.-W., Park, J.-H., Shim, H.-M., Koo, K.-K., 2013. Effect of amphiphilic additives on nucleation of hexahydro-1,3,5-trinitro-1,3,5-triazine. Cryst. Growth Des. 13 (11), 4688–4694.
Laval, P., Salmon, J.-B., Joanicot, M., 2007. A microfluidic device for investigating crystal nucleation kinetics. J. Cryst. Growth 303, 622–628.
Lindenberg, C., Mazzotti, M., 2010. Continuous precipitation of L-asparagine monohydrate in a micromixer: estimation of nucleation and growth kinetics. AIChE J. 57 (4), 942–950.
Mazutis, L., Griffiths, A.D., 2012. Selective droplet coalescence using microfluidic systems. Lab Chip 12, 1800–1806.
Parmentier, D., Bertrand, M., Plasari, E., Baron, P., 2013. Method to study the primary nucleation for solid solution: application to uranium-neodymium oxalate coprecipitation. Cryst. Struct. Theory Appl. 02 (2), 75–87.
Pound, G.M., La Mer, V.K., 1952. Kinetics of crystalline nucleus formation in supercooled liquid Tin. J. Am. Chem. Soc. 74 (9), 2323–2332.
Roelands, C.P.M., Horst, J.H., ter, Kramer, H.J.M., Jansens, P.J., 2006. Analysis of nucleation rate measurements in precipitation processes. Cryst. Growth Des. 6 (6), 1380–1392.
Sarrazin, F., Prat, L., Di Miceli, N., Cristobal, G., Link, D.R., Weitz, D.A., 2007. Mixing characterization inside microdroplets engineered on a microcoalescer. Chem. Eng. Sci. 62, 1042–1048.
Sear, R.P., 2014. Quantitative studies of crystal nucleation at constant supersaturation: experimental data and models. Cryst. Eng. Commun. 16, 6506–6522.
Shim, J.-U., Cristobal, G., Link, D.R., Thorsen, T., Fraden, S., 2007. Using microfluidics to decouple nucleation and growth of protein crystals. Cryst. Growth Des. 7 (11), 2192–2194.
Sollier, E., Murray, C., Maoddi, P., Di Carlo, D., 2011. Rapid prototyping polymers for microfluidic devices and high pressure injections. Lab Chip 11 (22), 3752–3765.
Söhnel, O., Garside, J., 1992. Precipitation: Basic Principles and Industrial Applications. Routledge, Oxford.
Teychene, S., Biscans, B., 2012. Crystal nucleation in a droplet based microfluidic crystallizer. Chem. Eng. Sci. 77, 242–248.
Toldy, A.I., Badruddoza, A.Z.M., Zheng, L., Hatton, T.A., Gunawan, R., Rajagopalan, R., Khan, S.A., 2012. Spherical crystallization of glycine from monodisperse microfluidic emulsions. Cryst. Growth Des. 12 (8), 3977–3982.
Wägli, P., Homsy, A., de Rooij, N.F., 2011. Norland optical adhesive (NOA81) microchannels with adjustable wetting behavior and high chemical resistance against a range of mid-infrared-transparent organic solvents. Sens. Actuators, B 156, 994–1001.
Weidinger, I., Klein, J., Stöckel, P., Baumgärtel, H., Leisner, T., 2003. Nucleation behavior of n-alkane microdroplets in an electrodynamic balance. J. Phys. Chem. B 107, 3636–3643.